

Naval Research Laboratory

Washington, DC 20375-5320

AD-A255 635



NRL/MR/4790-92-7110

②

Conditioning Electron Beams in the Ion-Focused Regime

R. F. FERNSLER, R. F. HUBBARD, AND S. P. SLINKER

*Beam Physics Branch
Plasma Physics Division*

September 17, 1992

DTIC
ELECTE
SEP 18 1992
S A D

256152
256152
256152

92 9 17 052

REPORT DOCUMENTATION PAGE			Form Approved OMB No. 0704-0188	
<small>Public reporting burden for this collection of information is estimated to average 1 hour per response, including the time for reviewing instructions, searching existing data sources, gathering and maintaining the data needed, and completing and reviewing the collection of information. Send comments regarding this burden estimate or any other aspect of this collection of information, including suggestions for reducing this burden, to Washington Headquarters Services, Directorate for Information Operations and Reports, 1215 Jefferson Davis Highway, Suite 1204, Arlington, VA 22202-4302, and to the Office of Management and Budget, Paperwork Reduction Project (0704-0188), Washington, DC 20503.</small>				
1. AGENCY USE ONLY (Leave blank)	2. REPORT DATE September 17, 1992	3. REPORT TYPE AND DATES COVERED Interim		
4. TITLE AND SUBTITLE Condition Electron Beams in the Ion-Focused Regime		5. FUNDING NUMBERS ARPA Order # 7781		
6. AUTHOR(S) R. F. Fernsler, R. F. Hubbard, and S. P. Slinker				
7. PERFORMING ORGANIZATION NAME(S) AND ADDRESS(ES) Naval Research Laboratory Washington, DC 20375-5320		8. PERFORMING ORGANIZATION REPORT NUMBER NRL/MR/4790-92-7110		
9. SPONSORING / MONITORING AGENCY NAME(S) AND ADDRESS(ES) DARPA Arlington, VA 22203 ONR Arlington, VA 22217		10. SPONSORING / MONITORING AGENCY REPORT NUMBER NSWC Silver Spring, MD 20903-5000		
11. SUPPLEMENTARY NOTES				
12a. DISTRIBUTION / AVAILABILITY STATEMENT Approved for public release; distribution unlimited.		12b. DISTRIBUTION CODE		
13. ABSTRACT (Maximum 200 words) <p>Relativistic electron beams propagating through dense gas are subject to the resistive hose instability, a virulent kink instability that restricts the effective range of high-current beams. Previous studies have shown that the instability can be suppressed by centering the beam and tailoring its emittance prior to injection into the gas. One means of centering and tailoring a beam is to use short "conditioning" cells that operate in the low-pressure, ion-focused regime. In this paper, analytic models are developed to understand and assess the performance of such cells.</p>				
14. SUBJECT TERMS Relativistic electron beam Ion-focused regime Resistive hose instability Emittance tailoring Beam conditioning			15. NUMBER OF PAGES 54	
			16. PRICE CODE	
17. SECURITY CLASSIFICATION OF REPORT UNCLASSIFIED	18. SECURITY CLASSIFICATION OF THIS PAGE UNCLASSIFIED	19. SECURITY CLASSIFICATION OF ABSTRACT UNCLASSIFIED	20. LIMITATION OF ABSTRACT UL	

CONTENTS

I.	INTRODUCTION	1
II.	RADIUS TAPERING IN A PASSIVE IFR CELL	4
	A. Equilibrium Model	4
	B. Beam Head Dynamics	8
	C. Emittance Growth from Anharmonic Pinching	10
III.	ENTRANCE AND EXIT FOILS	12
	A. Foil Heating	12
	B. Foil Focusing	12
	C. Space-Charge Depression	14
IV.	PARAMETER VARIATIONS IN A PASSIVE IFR CELL	16
	A. Design Equations	16
	B. Examples and Comparison with Simulation	20
V.	BEAM CENTERING	22
	A. Passive IFR Cell	22
	B. Centering in an Active IFR Cell	24
VI.	PLASMA MOTION	28
	A. Ion Channel Contraction and Expansion	28
	B. Ion Hose Instability	29
	C. Ion-Impact Ionization	30
	D. Trapping of Plasma Electrons	33
VII.	CONCLUSIONS	35
	ACKNOWLEDGEMENTS	36
	REFERENCES	37
	APPENDIX: Detuning the Resistive Hose Instability	49

CONDITIONING ELECTRON BEAMS IN THE ION-FOCUSED REGIME

I. INTRODUCTION

The ion-focused regime (IFR) offers several advantages for propagating and transporting intense, relativistic electron beams.¹⁻³ Chief among these is the ability to propagate in a self-pinched state free from interactions with destabilizing plasma electrons. Such propagation occurs when the beam travels through a plasma less dense than the beam. The radial electric field of the beam expels the plasma electrons, leaving the heavy positive ions to confine the beam electrostatically. The plasma can be created using the beam to ionize a background gas,²⁻¹⁰ or using a laser¹⁰⁻¹⁹ or a pre-existing low-energy electron beam¹⁹⁻²¹ for ionization. The first approach is termed "passive" IFR, while the latter two approaches using external ionization are termed "active" IFR. In either case, the gas must be sufficiently rarefied that the plasma electrons can escape without colliding with and further ionizing the gas molecules.⁴

Several IFR applications have already been employed. One application is to transport intense beams over long distances without external magnets. IFR transport over distances exceeding 80 m on laser-produced channels has been demonstrated on the Advanced Test Accelerator (ATA) at Lawrence Livermore National Laboratory^{13,14} and on the EPOCH facility at Sandia National Laboratories.¹⁶ Both of these facilities used an excimer laser to ionize a trace organic gas. A second application is suppression of beam instabilities in an induction accelerator. IFR transport on ATA allowed the solenoidal magnetic field to be turned off throughout most of the

accelerator, resulting in a factor of 3-5 increase in the amount of beam power that could be delivered without disruption from the beam-breakup instability.^{13,14} Other IFR applications include beam extraction from foilless diodes,^{18,19} beam confinement^{19,22} and extraction²³ in cyclic accelerators, and final focus in linear colliders.²⁴

In this paper, we consider yet another IFR application: namely, to prepare or "condition" a high-current beam prior to its injection into a dense gas. Experiments have demonstrated that an unconditioned beam straight from an accelerator or diode is disrupted by the resistive hose instability after propagating only a short distance in the gas.^{25,26} One strategy for combating this instability is to center the beam and reduce the transverse displacements that seed the instability.^{8,26-29} A second strategy is to tailor the beam emittance so that it decreases from head to tail. Such tailoring detunes the instability and can reduce hose growth substantially.^{8,25-34} In general, both centering and tailoring are needed to propagate intense beams over long distances in dense gas.

The IFR mode can be used for both centering and tailoring. Preionized IFR channels are especially effective at beam centering.¹²⁻¹⁴ Centering can also be achieved using passive IFR in a narrow pipe, as was first demonstrated on the Experimental Test Accelerator (ETA) at Lawrence Livermore National Laboratory⁶ and later on the SuperIBEX facility at the Naval Research Laboratory.³⁵ Passive IFR in a large pipe does little centering but tapers the beam radius. The radius taper can be converted to emittance tailoring by passing the beam through a final, thick scattering foil. This approach was first used on ETA³⁶ and has been the primary emittance tailoring technique for propagation experiments on ATA⁸ and

SuperIBEX.^{26,27} Passive IFR tailoring has also been employed at Sandia National Laboratories.³⁴

Although IFR conditioning has been shown to improve beam propagation dramatically, detailed IFR analysis has been lacking. In this paper, we develop and refine analytic models and design formulas for assessing the utility and limitations of the ion-focused regime in conditioning intense laboratory beams. Support for this work is given in another paper³⁷ that presents fully electromagnetic, particle simulations of IFR conditioning.

Analytical models of IFR propagation have been developed by a number of investigators.^{3,4,25,38-40} Here we concentrate on beam centering and radius tailoring. IFR radius tailoring is modeled by extending the equilibrium analysis of Briggs³ to include: emittance growth in the IFR, the role of the foils used at the transitions into and out of the IFR, and better treatment of the non-equilibrium beam head. Beam centering is analyzed in terms of the deflection forces produced on a beam by an ion channel and the container walls, and the growth in emittance caused by these forces. We conclude that under proper conditions, active IFR cells are effective at centering while passive IFR cells are effective at tailoring. Limitations from ion-channel collapse, the ion hose instability, ion-impact ionization, and magnetic trapping of the plasma electrons are discussed as well. Not discussed are effects like gas scattering and Ohmic erosion of the beam head³⁸ which are usually unimportant for laboratory applications.

ERIC QUALITY INSPECTED

Accession For	
NTIS CRA&I	<input checked="checked" type="checkbox"/>
DTIC TAB	<input type="checkbox"/>
Unannounced	<input type="checkbox"/>
Justification	
By	
Distribution/	
Availability Codes	
Dist	Avail and/or Special
A-1	

II. RADIUS TAPERING IN A PASSIVE IFR CELL

A. Equilibrium Model

Briggs³ developed a simple model for predicting the equilibrium radius $a_b(\tau)$ of a beam that creates its own IFR channel through beam impact ionization. Here we extend that model by allowing the beam current, emittance, and energy to vary with time τ into the beam pulse. We make the following assumptions: (i) the beam is highly relativistic with a Lorentz factor $\gamma \gg 1$; (ii) the plasma electrons are created solely through beam impact ionization and are ejected instantaneously; (iii) the plasma ions are immobile; (iv) the radial profile of the beam density is flat out to radius a_b ; and (v) a_b decreases with τ . The assumption that the beam profile is flat-topped (and therefore self-similar) is not rigorously justified but greatly simplifies the analysis without seriously compromising its validity. For consistency, we retain this assumption throughout most of the analysis. The assumption that the plasma electrons are collisionless has been studied by Yu⁴¹ and discussed by Buchanan.³⁸ In general, the assumption is valid at gas densities below a critical value, given³⁸ in room-temperature air by $P_c(\text{torr}) \approx (I_b/10 \text{ kA})(1 \text{ cm}/a_b)$. Effects from ion motion and magnetic trapping of plasma electrons are discussed in Sec. VI. Finally, because we are mainly interested in experimental applications where the gas density and propagation distance are small, we neglect gas scattering and Ohmic erosion.³⁸

Given our model assumptions, plasma ions are created according to

$$\frac{\partial n_i}{\partial \tau} = v_i n_b, \quad (1)$$

where n_b and n_i are the beam and ion densities, respectively, and v_i is the

rate at which the beam ionizes the gas. The rate ν_i is proportional to the density and atomic number of the gas, but depends only weakly on the beam energy for $\gamma \gg 1$; in room-temperature air, $\nu_i \approx P(\text{torr}) \text{ ns}^{-1}$. For a flat-topped collapsing beam, we can rewrite Eq. (1) in terms of the volumetric charge-neutralization fraction, $f_i = n_i/n_b$, as

$$\begin{aligned} \frac{\partial f_i}{\partial \tau} &= \frac{\partial}{\partial \tau} (n_i/n_b) = \nu_i - f_i \frac{\partial}{\partial \tau} \ln(n_b) \\ &= \nu_i - f_i \frac{\partial}{\partial \tau} \ln(I_b/a_b^2) . \end{aligned} \quad (2)$$

Here $I_b = e c \pi a_b^2 n_b$ is the beam current. The plasma electrons are neglected because they have been driven outside the beam.

We eliminate the dependence on a_b by combining the definition of normalized rms beam emittance,

$$\epsilon_n = \gamma a_b \sqrt{\frac{T_\perp}{\gamma m c^2}} , \quad (3)$$

with the radial pinch condition for the average beam temperature,^{1,42}

$$T_\perp = e f_i I_b / 2c . \quad (4)$$

Equation (3) assumes a flat-topped beam and neglects radial variations in γ , while Eq. (4) neglects self-forces to order $\gamma^{-2} \ll f_i$ and balances beam pressure against the ion pinch force. For a flat-topped beam, the rms radius a_{rms} and half-current radius $a_{1/2}$ are related by $a_{\text{rms}} = a_{1/2} = a_b / \sqrt{2}$. Although most results are given in terms of a_b , some results are given for convenience in terms of a_{rms} . Simulation³⁷ and experimental^{8,9} results commonly use $a_{1/2}$.

Combining Eqs. (3) and (4) produces

$$a_b^2 = 2\epsilon_n^2 I_A / \gamma f_i I_b , \quad (5)$$

where $I_A = mc^3/e \approx 17$ kA is termed the Alfven constant. (The Alfven current is traditionally defined⁴³ as I_A times the Lorentz factor $\beta\gamma$.)

Inserting Eq. (5) into Eq. (2) yields

$$\frac{\partial}{\partial \tau} f_i + f_i \frac{\partial}{\partial \tau} \ln(I_b \sqrt{\gamma} / \epsilon_n) = v_i / 2 . \quad (6)$$

This can be immediately integrated to yield

$$f_i(\tau) = \frac{v_i}{2} \frac{\epsilon_n}{\sqrt{\gamma} I_b} \int_0^\tau d\tau' \frac{\sqrt{\gamma} I_b}{\epsilon_n} . \quad (7)$$

Inserting Eq. (7) into force-balance equation (5) produces

$$a_b^{-2}(\tau) = \frac{v_i}{4} \frac{\sqrt{\gamma}}{\epsilon_n} \int_0^\tau d\tau' \frac{\sqrt{\gamma} I_b}{\epsilon_n I_A} . \quad (8)$$

Observe that no assumption has been made regarding how or when the emittance ϵ_n was generated.

Result (8) is based on the assumption of equilibrium, which is usually justified only if the IFR cell is long,

$$z \geq 0.5 \lambda_\beta = \pi a_b \sqrt{\gamma I_A / 2 f_i I_b} , \quad (9)$$

where λ_β is a betatron oscillation wavelength. Early in the beam head, condition (9) is not satisfied because $f_i I_b \rightarrow 0$. As a consequence, result (8) overestimates the degree of radius tailoring actually achievable. A correction is given in the next section.

The equations for f_i and a_b simplify if ϵ_n and γ are constant. In that case, Eq. (7) reduces to

$$f_i(\tau) = 0.5 v_i Q_b(\tau) / I_b(\tau) , \quad (10a)$$

while Eq. (8) reduces to

$$a_b(\tau) = \frac{2\epsilon_n}{\sqrt{\gamma v_i Q_b(\tau) / I_A}} . \quad (10b)$$

Here the time-dependent beam charge is given by

$$Q_b(\tau) = \int_0^\tau d\tau' I_b(\tau') . \quad (11)$$

Result (10b) demonstrates that radius tailoring, $\partial a_b / \partial \tau < 0$, occurs as Q_b increases monotonically with time τ . For example, if I_b rises as τ^m , the charge and radius vary as $Q_b \propto \tau^{m+1}$ and $a_b \propto \tau^{-(m+1)/2}$, respectively. Briggs,³ result, $a_b \propto \tau^{-1/2}$, is recovered by setting $m = 0$.

Another useful example is a beam current that rises and falls as a half-sine wave,

$$I_b(\tau) = I_0 \sin(\pi\tau/\tau_p) \quad (12a)$$

where I_0 is the peak current and τ_p is the pulse duration. Then,

$$a_b(\tau) \propto [1 - \cos(\pi\tau/\tau_p)]^{-1/2} . \quad (12b)$$

The beam thus pinches rapidly at early τ but levels off at late τ . In this

case, the neutralization fraction becomes large, $f_i \gg 1$, as $\tau \rightarrow \tau_p$. Once f_i exceed unity, the plasma electrons are no longer ejected but are pulled back by the plasma ions. Nevertheless, the analysis remains approximately valid because the plasma electrons ejected earlier oscillate at large radius about the ion column, rather than re-concentrating within it. As a consequence, the pinch force on the beam is still largely controlled by the ion line density $f_i I_b / c$.

B. Beam Head Dynamics

The preceding model is valid for those portions of the beam that have attained equilibrium, but it is not valid for the weakly-pinched beam head. A simple correction is to assume free expansion in the head and equilibrium in the body. This composite model provides a good estimate for the maximum head-to-tail radius variation produced from a passive IFR cell. A more accurate approach would be to solve the Lee-Cooper envelope equation.⁴⁴

We compute the radius of the freely expanding beam head by assuming that the beam is injected with a Maxwellian thermal distribution determined by the initial emittance ϵ_0 and rms radius $r_h(0)$. The unpinched head then evolves to a Gaussian profile expanding at a constant rate:⁴⁴

$$r_h(z) \rightarrow \frac{\epsilon_0 z}{\gamma r_h(0)} . \quad (13)$$

Here z is the propagation distance, and we have assumed $r_h(z) \gg r_h(0)$. We multiply the rms radius r_h by $\sqrt{2}$ to compute the corresponding edge radius for the flat-topped profile assumed in the model. Free-expansion and wall scrape-off thus restrict the edge radius to

$$a_b(\tau, z) \leq a_{\max} \equiv \text{Min}\{b, 2z\varepsilon_0/\gamma a_0\}, \quad (14)$$

where b is the pipe radius and $a_0 = \sqrt{2}r_h(0)$ is the initial edge radius.

Restriction (14) shows that the radius of the early beam head varies with z but not τ , assuming constant $\varepsilon_0/\gamma a_0$. In this region, the solution to Eq. (2) is $f_i(\tau) = v_i Q_b(\tau)/I_b(\tau)$, twice the value given in Eq. (10a) for a collapsing beam. This additional growth raises f_i in the equilibrium region, so that Eq. (10a) should be replaced with

$$\begin{aligned} f_i I_b &= 0.5 v_i [Q_b(\tau) - Q_b(\tau_i)] + f_i(\tau_i) I_b(\tau_i) \\ &= 0.5 v_i [Q_b(\tau) + Q_b(\tau_i)] \end{aligned} \quad (15a)$$

in the equilibrium zone, $\tau \geq \tau_i$. To incorporate this change, we insert Eq. (15a) into Eq. (5) to obtain a first-order revision to Eq. (10b):

$$\begin{aligned} a_b(\tau) &= \frac{2\varepsilon_0}{\sqrt{\gamma v_i [Q_b(\tau) + Q_b(\tau_i)]/I_A}} \\ &= \frac{2\varepsilon_0}{\sqrt{[\gamma v_i Q_b(\tau)/I_A] + (\gamma a_0/z)^2}}. \end{aligned} \quad (15b)$$

Here we have ignored beam scrape-off and have normalized $a_b(0)$ to the free-expansion limit, $2z\varepsilon_0/\gamma a_0$. This approximation applies to both the pinched and unpinched regions of the beam. The transition time τ_i to equilibrium is given by

$$v_i Q_b(\tau_i) = (a_0/z)^2 \gamma I_A. \quad (16)$$

C. Emittance Growth from Anharmonic Pinching

Result (8) demonstrates that temporal variations in $\epsilon_n/\sqrt{\gamma}$ alter the radius tailoring obtained from a passive IFR cell. In this section we show that the IFR cell itself changes the emittance. We conclude from this calculation that a passive IFR cell produces radius tailoring only if the beam is injected warm, $T_{\perp} > 0$. If the beam enters cold, it exits with little radius tailoring but with the emittance inverse tailored, $\partial\epsilon_n/\partial\tau > 0$. As discussed in the appendix, such a beam is predicted to be highly hose unstable when injected into dense gas.

A simple estimate of emittance growth for an initially cold beam is as follows.⁴⁵ If the IFR pinch force is harmonic, each beam electron undergoes sinusoidal motion so that its time-averaged rms radius contracts by $1/\sqrt{2}$. At the same time, the rms radial velocity of each electron rises from zero to $r_0\omega_\beta/\sqrt{2}$, where r_0 is the injection radius and ω_β is the oscillation frequency. For a uniform ion channel,

$$\omega_\beta = \frac{c}{a_b} \sqrt{2f_i I_b / \gamma I_A} . \quad (17)$$

In general, the beam and ion channel are not flat-topped, so the pinch force is not harmonic. The electrons then do not oscillate at the same frequency, and they become out of phase with one another. As orbit coherence is lost, the beam electrons thermalize to a steady rms radius and transverse thermal velocity given, according to the above analysis, by $r_{bo}/\sqrt{2}$ and $r_{bo}\omega_\beta/\sqrt{2}$, respectively, where r_{bo} is the rms radius at injection and ω_β is an average oscillation frequency. This suggests that the normalized emittance of a beam in a fixed, anharmonic centering force evolves via phase-mixing to a value no smaller than

$$\epsilon_n^{(min)} \approx 0.5 \gamma r_{bo}^2 \omega_\beta / c . \quad (18)$$

This result may also be derived by relating the final transverse beam temperature to the work done by the pinch force in contracting the beam.⁴⁶ The latter approach is particularly useful if the pinch force is highly anharmonic.

Result (18) and the discussion preceding it indicate that a passive IFR cell does not produce radius tailoring in an initially cold beam. Instead, the beam contracts uniformly by $1/\sqrt{2}$, and its emittance rises with τ as $f_i I_b$ rises. To produce radius tailoring, the beam should be preheated so that the initial emittance ϵ_0 satisfies

$$\epsilon_0 > \epsilon_n^{(\min)}. \quad (19a)$$

To produce head expansion, the emittance should additionally satisfy

$$\epsilon_0 > \gamma a_0^2 / \sqrt{8} z. \quad (19b)$$

According to Eq. (15b), radius tailoring will then occur up to a time $\tau_e > \tau_i$, where τ_e is defined by

$$v_i Q_b(\tau_e) = [8(\epsilon_0 / \gamma a_0)^2 - (a_0 / z)^2] \gamma I_A. \quad (20)$$

For $\tau \geq \tau_e$, the radius remains roughly constant at $a_b \approx a_0 / \sqrt{2}$, and the emittance ϵ_n grows as the ion pinch strength increases according to

$$\begin{aligned} f_i I_b &= f_i(\tau_e) I_b(\tau_e) + v_i [Q_b(\tau) - Q_b(\tau_e)] \\ &= v_i [Q_b(\tau) - 0.5 Q_b(\tau_e) + 0.5 Q_b(\tau_i)] . \end{aligned} \quad (21)$$

III. ENTRANCE AND EXIT FOILS

A. Foil Heating

IFR cells usually require entrance and exit foils to maintain the necessary gas pressure. These foils scatter the beam and increase its angular divergence by⁴⁷

$$\langle \theta^2 \rangle = \langle \theta_i^2 \rangle + k_f t_f / \gamma^2 . \quad (22)$$

Here $\langle \theta_i^2 \rangle$ characterizes the initial angular spread of the beam, t_f is the foil thickness, and k_f is a scattering coefficient that depends on the foil material. Foil scattering thus raises the normalized mean-squared beam emittance, $\epsilon_n^2 = 0.5 \gamma^2 a_b^2 \langle \theta^2 \rangle$, by

$$\epsilon_n^2 = \epsilon_i^2 + 0.5 k_f t_f a_b^2 , \quad (23)$$

where ϵ_i is the initial emittance. Because k_f is nearly independent of the beam energy or current, foil scattering can serve as a convenient means for producing constant emittance in a pencil beam; see Sec. IV-A for further discussion. For beam energies of several MeV, $k_f \approx 1$ for t_f expressed in equivalent mils of titanium.

B. Foil Focusing

A foil in the path of an intense electron beam quickly becomes conducting, thereby shorting the electrostatic repulsive field of the beam.⁴⁸⁻⁵⁰ This momentary shorting imparts a focusing impulse much like a thin lens. For paraxial beams, the foil focal length varies as⁵⁰

$$f_\ell = g_f a_{\text{rms}} \frac{\gamma I_A}{(1-f_i) I_b}, \quad (24)$$

where a_{rms} is the rms beam radius, $g_f \sim 0.4$ is a geometrical coefficient determined by the beam radial profile and wall radius, and f_i is the gas charge-neutralization fraction averaged over the two sides of the foil.

Foil focusing has little effect if it is weak,

$$f_\ell \gtrsim \lambda_\beta/4, \quad (25)$$

or if the IFR cell is short,

$$f_\ell \gg z. \quad (26)$$

Here λ_β is the IFR betatron wavelength given in Eq. (9). Condition (26) is always met if

$$I_b/\gamma I_A \ll a_o/z. \quad (27)$$

If none of these conditions is met, the beam is over-focused and some electrons are pushed to outside a_o . This increases the effective injection radius, and it adds beam wings to the radial profile. The over-focusing can also produce loss of transported current as the beam scrapes the pipe walls. All of these effects are strongest near the peak of I_b .

Another adverse foil effect is that the focal length f_ℓ varies with particle position. This anharmonic focusing raises the beam emittance by⁵⁰

$$\epsilon_n^2 \rightarrow \epsilon_n^2 + [\alpha_f(1-f_i)a_{\text{rms}} I_b/I_A]^2, \quad (28)$$

where $\alpha_f \sim 0.1-0.5$ is a geometrical coefficient determined by the beam profile and pipe diameter. Foil focusing thus produces inverse emittance tailoring during the rising portion of the beam current. Such inverse tailoring must be eliminated to produce radius tailoring. The simplest solution is to make the entrance foil sufficiently thick that emittance growth from scattering dominates the growth from anharmonic focusing. This requires, according to Eqs. (23) and (28), a foil thickness satisfying

$$k_f t_f \gg [\alpha_f(1-f_i)I_b/I_A]^2. \quad (29)$$

One can show that this is compatible with the emittance required in Eq. (20) provided

$$I_b/\gamma I_A \ll f_i/2\alpha_f^2. \quad (30)$$

In general, foil focusing can be disregarded if the beam is highly paraxial, $I_b \ll \gamma I_A$.

C. Space-Charge Depression

Foil focusing stems from charge induced on the foil. This charge not only shorts the radial electric field, but it also produces an axial electric field. We show here that the axial field, not the radial field,⁴³ is responsible for space-charge depression of the beam energy.

As a beam leaves a conducting foil, it decelerates in response to the (image) charge on the foil. The induced axial field is electrostatic and given by $E_{zf} = -\partial\phi_f/\partial z$, where ϕ_f is the potential from the foil charge. The field E_{zf} lowers the beam energy by

$$\Delta(\gamma mc^2) = e \int_0^\infty dz \int_0^b dr \frac{\partial i_b}{\partial r} \frac{\partial \phi_f}{\partial z} . \quad (31)$$

Here $i_b(r)$ is the fraction of beam current within radius r , and $z = 0$ is the foil location. The foil potential ϕ_f satisfies Laplace's equation outside the foil and is given on the foil by the neutralization requirement

$$\frac{\partial \phi_f}{\partial r} = E_{ro} \quad (32)$$

where E_{ro} is the radial electric field from the beam and IFR plasma.

The foil fields affect the beam over $\Delta z \sim 3a_{rms}$ outside the foil.⁵⁰ If $f_\ell \gg 3a_{rms}$, the beam profile can be taken as constant in z , and the order of integration in Eq. (31) can be interchanged to yield

$$\begin{aligned} \Delta(\gamma mc^2) &= e \int_0^b dr \frac{\partial i_b}{\partial r} \int_0^\infty dz \frac{\partial \phi_f}{\partial z} \\ &= - e \int_0^b dr \frac{\partial i_b}{\partial r} \phi_f(r, 0, t) \\ &= e \int_0^b dr i_b E_{ro} \\ &= - \int_0^b dr \frac{2e i_b^2}{rc} (1 - \bar{f}) I_b . \end{aligned} \quad (33)$$

Here we have integrated by parts, applied boundary condition (32) plus the condition that $\phi_f = 0$ at $r = b$ and $z = \infty$, imposed $i_b = 0$ at $r = 0$, and expressed E_{ro} in terms of an average neutralization fraction, $1 - \bar{f}(r)$. For

a flat-topped beam in vacuum, result (33) reduces to $\Delta\gamma = -[\ln(b^2/a_b^2)+0.5](I_b/I_A)$. One can show that this is just the energy needed to regenerate the beam self-fields (magnetic and electrostatic) outside the foil.

Although the energy loss $\Delta\gamma$ is eventually recovered as the beam passes through the IFR exit foil, the value of γ within the IFR cell remains reduced. This alters the radius tailoring because γ varies with time τ (and with radius r because E_{zf} varies with r). These effects become pronounced for $\Delta\gamma \rightarrow -(\gamma_0-1)$, where γ_0 is the injection energy. This value of $\Delta\gamma$ defines the space-charge limiting current⁴³ in the IFR cell. Above this current, the beam slows and expands to fill the pipe, until scrape-off or low axial velocity reduces I_b .

IV. PARAMETER VARIATIONS IN A PASSIVE IFR CELL

A. Design Equations

In this section, we use the previous results to construct a set of algebraic equations for designing a passive IFR tailoring cell for a given beam. For simplicity, we ignore space-charge depression and foil focusing (valid for highly paraxial beams), and we assume that the beam approaches the IFR cell with constant energy γ , emittance ϵ_i , and radius a_0 . The adjustable IFR parameters are the entrance and exit foil thicknesses, the cell dimensions b and z , and the gas composition and pressure P . The output is a prescribed variation in the beam radius given as follows: a_b is to start collapsing at time τ_i , fall until time τ_e , and saturate at $a_0/\sqrt{2}$ for $\tau \geq \tau_e$. The time τ_i marks the transition from free expansion to

pinched equilibrium, and the time τ_e is where emittance growth prevents further beam collapse. The actual transitions at τ_i and τ_e are, of course, gradual rather than abrupt.

The output beam temperature is specified in terms of a maximum value, T_{\max} , the choice of which is discussed later. This bound limits the IFR pinch strength to

$$f_i I_b \leq I_{\max} = 2cT_{\max}/e, \quad (34)$$

according to Eq. (4). Here I_{\max} is an equivalent pinch "current" characterizing the strength of the ion charge seen by the beam. Because $f_i I_b$ increases monotonically with time, it reaches I_{\max} at the end of the beam pulse, $\tau = \tau_p$. Applying this bound to Eq. (21) yields

$$v_i = I_{\max} / [Q_b(\tau_p) - 0.5Q_b(\tau_e) + 0.5Q_b(\tau_i)] . \quad (35)$$

This equation specifies the gas ionization rate v_i , and thus the gas pressure P , in terms of the maximum ion pinch "current" I_{\max} and the beam charge Q_b at the times τ_i , τ_e , and τ_p .

We now compute the thickness of the IFR entrance foil. The beam radius at time τ_e equals $a_0/\sqrt{2}$. To produce this radius, Eqs. (15b) and (16) indicate that the beam emittance should satisfy

$$\varepsilon_0 = a_0 \sqrt{\gamma v_i [Q_b(\tau_e) + Q_b(\tau_i)] / 8I_A} . \quad (36)$$

According to Eq. (23), the entrance foil thickness should therefore satisfy

$$k_f t_f = \gamma v_i [Q_b(\tau_e) + Q_b(\tau_i)] / 4I_A - 2(\varepsilon_i/a_0)^2, \quad (37a)$$

where the original beam emittance is assumed to be small, $\epsilon_i < \epsilon_o$. We can rewrite condition (37a) using Eq. (35) as

$$k_f t_f = \frac{\gamma I_{\max}}{2I_A} \left(\frac{Q_b(\tau_e) + Q_b(\tau_i)}{2Q_b(\tau_p) - Q_b(\tau_e) + Q_b(\tau_i)} \right) - 2 \left(\frac{\epsilon_i}{a_o} \right)^2. \quad (37b)$$

The length z of the IFR cell determines the amount of radius tailoring achieved and its onset time τ_i . The length is given from Eqs. (16) and (35) by

$$z = a_o \left(\frac{\gamma I_A}{I_{\max}} \right)^{1/2} \left(\frac{Q_b(\tau_p) - 0.5 Q_b(\tau_e) + 0.5 Q_b(\tau_i)}{Q_b(\tau_i)} \right)^{1/2}. \quad (38)$$

The use of larger z would lower τ_i and give more tailoring. We point out that result (38) is consistent with equilibrium requirement (9) at the tailoring-end time τ_e only if

$$a_{\max}/a_{\min} \geq \pi, \quad (39)$$

where the minimum output radius $a_{\min} = a_o/\sqrt{2}$.

The maximum head-to-tail radius variation is given by

$$\frac{a_{\max}}{a_{\min}} = \sqrt{\frac{Q_b(\tau_e) + Q_b(\tau_i)}{Q_b(\tau_i)}}. \quad (40)$$

If desired, one could specify a_{\max}/a_{\min} as a design objective in place of τ_i , and use Eq. (40) to calculate $Q_b(\tau_i)$. In any event, the pipe radius b is chosen to minimize beam scrape-off:

$$b > a_{\max} = a_o \sqrt{\frac{Q_b(\tau_e) + Q_b(\tau_i)}{2Q_b(\tau_i)}}. \quad (41)$$

Pipe scrape-off could, of course, be used to control the head radius a_{\max} and tailoring-onset time τ_i , but only at the loss of current in the head.

Equations (35), (37), (38), and (40) are a prescription for designing an IFR radius tailoring cell. To convert the radius tailoring to emittance tailoring, the beam must be further heated at the IFR exit to a constant temperature, $T_f \geq T_{\max}$. Emittance tailoring is maximized when $T_f \gg T_{\max}$ so that $\epsilon_n(\tau)$ varies directly with $a_b(\tau)$. According to Eqs. (23) and (34), this can be achieved by passing the beam through a scattering foil whose thickness t_f satisfies

$$k_f t_f = 2\gamma T_f / mc^2 \gg \gamma I_{\max} / I_A . \quad (42)$$

The beam could alternatively be heated using an active IFR cell or similar anharmonic centering scheme. The IFR exit foil should then be thin.

The final emittance desired for the beam determines T_f . To keep the radius of the beam body unchanged in the propagation region following the IFR cell, we set

$$T_f = eI_{\text{eff}}/2c , \quad (43)$$

where I_{eff} is the effective body pinch current in the propagation region. For a beam propagating in dense gas, I_{eff} equals the beam current minus the plasma return current enclosed by the beam; in this case, I_{eff} typically⁵¹ lies between half to one times the peak beam current I_0 . Choice (43) matches the beam body but not the head. As a consequence, the overheated head will expand as the beam propagates. The head mismatch can be reduced by raising the IFR gas pressure P , but this decreases the amount of

emittance tailoring achieved. At times $\tau > \tau_e$, the emittance is always slightly inverse tailored.

Before closing this section, we point out that the design formalism is based on the assumption that the beam should taper to its smallest possible radius, $a_0/\sqrt{2}$. In some instances, however, a larger minimum may be desired, e.g., to propagate a beam stably over long distances outside the IFR cell. In that case, design equations (35), (38), and (41) can be retained by setting τ_e equal to the pulse duration τ_p . But Eq. (36) for the entrance emittance should be replaced with $\epsilon_n = a_{\min}(\gamma I_{\max}/2I_A)^{1/2}$, where a_{\min} is the desired minimum beam radius at time τ_p .

B. Examples and Comparison with Simulation

In this section we illustrate the radius variation produced by a passive IFR cell. The beam is assumed to have the half-sine current form given by Eq. (12a), with nominal parameters $I_0 = 17$ kA, $a_0 = 1$ cm, $\epsilon_i = 0.3$ rad-cm, $\gamma_0 = 10$, and $\tau_p = 40$ nsec. Let us design the IFR cell to produce a tailoring onset time $\tau_i = 4$ ns, a tailoring end time $\tau_e = \tau_p = 40$ ns, and a peak ion-channel strength $I_{\max} = 2.2$ kA. Using the fact that $Q_b(\tau) = (I_0 \tau_p / \pi)[1 - \cos(\pi \tau / \tau_p)]$, we compute the necessary gas ionization rate from Eq. (35) as $v_i = 10^7 \text{ s}^{-1}$, corresponding to a gas pressure $P = 10$ mtorr in air. Equation (37b) indicates that the IFR entrance foil should be 0.5 mil of titanium, corresponding to a net injection emittance of $\epsilon_0 = 0.6$ rad-cm. Equation (38) indicates the cell should be 40 cm long, and scrape condition (41) indicates that the wall radius b should exceed 5 cm. We set $b = 10$ cm for operational flexibility. These beam and IFR cell parameters are similar to those used in the SuperIBEX experiments.⁹

The predicted beam radius $a_b(\tau)$ at cell exit is given by Eq. (15b), subject to the collapse restriction, $a_b \geq a_0/\sqrt{2}$. Although foil focusing is predicted to be strong for this beam, we ignore it here. The effect is incorporated, however, in the simulations described in Ref. 37.

Figure 1 plots $a_b(\tau)$ from Eq. (15b) for several values of the IFR gas pressure P . The pressure P affects both the tailoring onset time τ_i and the end time τ_e , but does not affect the head radius a_{\max} . The latter is limited by free expansion to $a_{\max} = 4.8$ cm in this case. Raising P shortens τ_i and τ_e so that the beam pinches more quickly. In the beam tail ($\tau > 30$ ns), the radius is roughly constant because the beam current decreases rapidly and little additional ionization is produced.

Figure 2 shows the effect of changing the input emittance ϵ_0 (the entrance foil thickness) while holding $P = 10$ mtorr. The emittance ϵ_0 affects the tailoring end time τ_e and the head radius a_{\max} , but does not affect the tailoring onset time τ_i . Little tailoring occurs if ϵ_0 is too low, and the beam does not pinch tightly if ϵ_0 is too high.

Figure 3 shows the effect of the cell length z on tailoring. The cell length affects both a_{\max} and τ_i but usually has little effect on τ_e . Consequently, raising z increases tailoring mainly in the beam head. In general, the cell should be made too long rather than too short to maximize tailoring flexibility.

In Fig. 4 we correct for space-charge depression of the beam energy using Eq. (33). The reduction in γ approaches 50% near peak current in Fig. 4a for the standard case described above. Nevertheless, the effect on radius tailoring is relatively modest, as shown by the comparison in Fig. 4b between the corrected beam radius (solid line) and the uncorrected radius (dashed line). However, if the current were to approach the space-

charge limiting value ~ 30 kA, the beam would expand to fill the pipe with the radius virtually untailored.

To test our model, we have compared its predictions with those from a fully electromagnetic particle code, FRIEZR.³⁷ In particle codes (and experiments), the beam profile rounds so that the half-current radius $a_{1/2}$ or rms radius a_{rms} is a more useful measure than the edge radius a_b . To allow for this difference, we divide the analytical result for a_b by $\sqrt{2}$, which is the appropriate scale factor for both $a_{1/2}$ and a_{rms} for a flat-topped beam. In Fig. 5, we plot the analytical radius $a_b/\sqrt{2}$ (dashed line) and the simulation radii, $a_{1/2}$ (solid line) and a_{rms} (dot-dashed line), for a beam injected with a Gaussian radial profile and the nominal parameters given above. The analytical result tracks $a_{1/2}$ fairly closely, especially for $\tau > 10$ ns. The discrepancy at early times occurs because the beam is not flat-topped and because it over-expands without equilibrating. Overall, the agreement between code and theory is good, indicating the utility as well as the limitations of the model.

V. BEAM CENTERING

A. Passive IFR Cell

Another major benefit of IFR propagation is suppression of azimuthal asymmetries like transverse offsets ($m=1$), non-circular profiles ($m=2$), and filamentation ($m > 2$). In all cases, the price of symmetrization is increased beam emittance. Here we concentrate on beam centering.

There are two types of centering forces from an IFR cell: those produced by the IFR channel itself, and those from the pipe walls. The

wall forces are easily computed if we assume that the pipe is perfectly conducting and that the ion channel is cylindrical and long, $b \partial/\partial z \ll 1$. The latter condition is usually well satisfied if the beam is paraxial and the IFR cell is long, $z \gg b$. The ion channel can then be treated as a long cylinder of line charge q_i . If the channel resides at a location displaced y_c from the pipe center, it induces a charge on the pipe that can be represented as an image line charge of $-q_i$ located at $(b/y_c)^2 y_c$ outside the pipe.⁵² This image charge deflects the beam with an average force given by

$$F_y = - \frac{2eq_i}{\left| (b/y_c)^2 y_c - y_b \right|^2} \left((b/y_c)^2 y_c - y_b \right), \quad (44)$$

where y_b is the beam centroid. Deflection forces from the beam image charge and current cancel to order γ^{-2} .

In a passive IFR cell, the channel is essentially centered on the beam, $y_c = y_b$, with a charge $q_i = v_i Q_b / c$. Equation (44) can then be written as

$$F_y = - \frac{2ev_i Q_b}{(b^2 - y_b^2)c} y_b. \quad (45)$$

For $y_b \ll b$, the centering force reduces to $F_y = (2ev_i Q_b / b^2 c) y_b$. This indicates that the beam centers in a characteristic distance

$$z_c = (\pi/2) \sqrt{\gamma I_A / 2v_i Q_b} b. \quad (46)$$

Phase mixing in the anharmonic pinch force from q_i damps subsequent oscillations in y_b .

Result (46) neglects any separation between the beam and ion channel. Such separation will in fact develop because the rise in Q_b with τ causes

the beam head to center more slowly than the body. This difference tilts the beam and causes the plasma channel to lag behind and separate, thereby generating additional beam deflection forces. Nevertheless, Eq. (46) provides a useful estimate for the minimum cell length needed to center a beam in a passive IFR cell.

IFR centering has been demonstrated using the SuperIBEX beam described earlier. The centering experiments were conducted in a pipe 114 cm long by 4.7 cm in diameter and filled with 20 mtorr of nitrogen.³⁵ Nearly all of the beam was centered by the pipe, as predicted by Eq. (46). The weakly pinched head, however, was lost to pipe scrape-off as expected.

B. Centering in an Active IFR Cell

In an active IFR cell, the channel is created externally and usually in the center of the pipe. A centered channel eliminates the wall force, as can be shown by setting $y_c = 0$ in Eq. (44). This leaves the channel to guide as well as pinch the beam.

Unlike wall centering, channel centering cannot be computed simply by evaluating the static, net deflection force on the beam. Instead, dynamical forces from orbit phase-mixing and beam distortion must be included as well. To illustrate this, consider a hollow beam surrounding a narrow channel. Because the beam produces no fields or forces within itself, there is no force on the enclosed channel, and thus there is no net deflection force on the beam by reciprocity. However, the beam does not maintain its original structure but collapses towards the channel. This collapse causes the beam to fill in and distort until it forms a new profile centered about the channel. This is a dynamical process that cannot be predicted using a static, rigid-rod force calculation.

In fact, narrow channels are especially effective at centering beams, hollow or not. The main reason is that the channel force is then highly anharmonic, causing the beam electrons to orbit about the channel but not in phase with one another. As a consequence, the orbits quickly lose coherence and phase-mix such that the non-rigid beam distorts into a new profile centered about the channel. Phase-mix centering can occur in distances as short as a few λ_β for a highly anharmonic force. A second reason narrow channels are effective at beam centering is that the full ion charge attracts each beam electron, thereby maximizing the channel force.

To illustrate beam centering in an active IFR cell, we consider a broad beam and a wire-like ion channel created externally with a fixed line charge q_i per unit length. The line charge q_i attracts each beam electron with a force

$$F_r(r) = -2eq_i/r, \quad (47)$$

where r is the radial distance from the channel. This force heats the electrons until pressure balance is achieved, $\partial(n_b T_\perp)/\partial r = n_b F_r$, where n_b is the beam density and T_\perp is the transverse beam temperature. Using pressure balance and Eq. (47), the average final temperature is given by

$$\begin{aligned} \langle T_\perp \rangle &= N_b^{-1} \int_0^b dr \, 2\pi r \, n_b T_\perp = -N_b^{-1} \int_0^b dr \, \pi r^2 \frac{\partial}{\partial r} (n_b T_\perp) \\ &= -N_b^{-1} \int_0^b dr \, \pi r^2 \, n_b F_r = eq_i N_b^{-1} \int_0^b dr \, 2\pi r n_b \\ &= eq_i, \end{aligned} \quad (48)$$

where $N_b = I_b/ec$ is the beam line density. Here we have integrated by parts and used the boundary condition $n_b = 0$ at $r \geq b$. Only for a wire-like force is $\langle T_{\perp} \rangle$ independent of the injection conditions.

Let us now consider an initially cold beam. As an electron travels from radius r to r' , the force F_r raises its transverse energy to

$$\frac{\gamma m v_r^2}{2} = \int_r^{r'} dr'' F_r(r'') = 2eq_i \ln(r/r') . \quad (49)$$

Solving for v_r allows us to compute the time taken for the electron to complete a round trip around the channel:

$$\begin{aligned} t_o(r) &= 4 \int_0^r \frac{dr'}{v_r} = 2 \sqrt{\gamma m / eq_i} \int_0^r \left[\ln(r/r') \right]^{-1/2} \\ &= 2 \sqrt{\pi \gamma m / eq_i} r . \end{aligned} \quad (50a)$$

The corresponding propagation distance is

$$\lambda_\beta(r) = ct_o(r) = 2\pi r (\gamma I_A / \pi c q_i)^{1/2} . \quad (50b)$$

All electrons thus gyrate about the channel, but they gyrate at different frequencies determined by their initial location r from the channel.

The variation in oscillation time causes the electrons to become out of phase with one another. As the particles lose coherence, the beam evolves to a smooth, stable distribution centered about the channel. That is, phase mixing of the particle orbits damps fluctuations in the beam profile and centroid location.¹² Without this damping, the fluctuations would persist, and the beam would forever oscillate about the channel. The

latter scenario occurs if the channel force is perfectly harmonic, $F_r(r) \propto r$, so that t_0 is independent of r . For this reason, a flat-topped ion channel broader than the beam is ineffective at beam centering.

Electrons starting far from the channel take longer to cross it, and thus they phase-mix more slowly than electrons starting near the channel. The characteristic distance for phase-mix centering is therefore governed by the longest betatron wavelength, given from Eq. (50b) by

$$\lambda_{\beta}^{\max} = 2(a_0 + y_b) \sqrt{\pi \gamma I_A / c q_i}, \quad (51)$$

where a_0 is the beam edge radius and y_b is the beam offset at injection. The beam first crosses the channel at $z_c = \lambda_{\beta}^{\max}/4$, but several λ_{β}^{\max} are needed for phase-mixing to damp subsequent oscillations of the centroid.

If the electrons are injected warm rather than cold, their tangential velocity causes the orbits to precess about the channel. This precession produces a beam that is azimuthally symmetric as well as centered. Asymmetries like beam filamentation and non-circularity are thereby removed.

Symmetrization and centering come at the expense of beam emittance. A lower bound for the emittance can be derived by combining temperature result (48) with an estimate for the final beam area, yielding

$$\epsilon_n^{\min} \approx (2\gamma c q_i / I_A)^{1/2} (a_0 + y_b). \quad (52)$$

This is consistent with Eqs. (17) and (18) for $y_b = 0$ and $f_i I_b = 2c q_i$. Note that the offset is unimportant unless it is large, $y_b \gtrsim a_0$.

An active IFR cell could be combined with a separate passive IFR cell to produce a beam that is both centered and emittance tailored. The most

efficient arrangement is to place the active IFR cell last, so that the heating from this cell eliminates the need for a final, thick scattering foil. In the reverse order, the emittance gained from the centering cell cannot be efficiently utilized.

A limitation of active IFR cells is that they do not become fully operational until the beam current rises above cq_1 . In the early beam head, this condition is not met, and the head propagates in an overdense plasma. This region is often sufficiently short, however, that there is little adverse impact on the beam.

VI. PLASMA MOTION

A. Ion Channel Contraction and Expansion

The assumption that the ions are stationary and the plasma electrons are instantaneously ejected is not, of course, strictly justified. In this and the following sections, we discuss ion pinching, ion hose motion, ion impact ionization, and magnetic trapping of the plasma electrons.

The beam electrostatically pinches the ion channel, causing it to contract. Such contraction takes place on an ion crossing time given by

$$\tau_c = (\pi a_0 / 2c) (M/m)^{1/2} (I_A / I_b)^{1/2}, \quad (53)$$

where M is the ion mass. Contraction is unimportant if τ_c is much larger than the beam pulse duration τ_p , or if the channel is narrow as was assumed in the analysis of an active IFR cell. If the channel is broad, its contraction raises the ion charge $f_i I_b / c$ seen by the beam; this raises the

equilibrium value of ϵ_n/a_b , as indicated by Eqs. (3) and (4). Using the arguments given for the beam, channel contraction is ultimately limited to $\sim 1/\sqrt{2}$, and a broad channel that contracts by this amount doubles $f_i I_b$ and causes ϵ_n/a_b to increase by $\sqrt{2}$. However, the contraction can be larger at $\tau = \tau_c$, depending on how anharmonic the channel pinch force is.

The main effect of channel contraction in a passive IFR cell is to raise ϵ_n if the tailoring-end time $\tau_e < \tau_c$, or to reduce τ_e if $\tau_e > \tau_c$. In either case, the effect is usually modest because the channel is being continuously created by the beam. Channel collapse is therefore generally unimportant in passive IFR cells, as well as in narrow-channel active IFR cells.

Late in the beam pulse, the beam current drops and the beam density ultimately falls below the ion density, $f_i > 1$. Thermal pressure and mutual repulsion then drive the ion channel to expand. Such expansion could cause the tail of the beam to flare, especially if the beam current decays over a time longer than an ion crossing time τ_c . In a typical passive IFR cell where $f_i \ll 1$ in the beam body, flaring is not expected until very late in the pulse. Tail flaring is similarly unimportant in active IFR cells provided the ion channel is initially much smaller than the beam. Expansion and contraction of the ion channel can, of course, be reduced by using a fill gas with a large ion mass M .

B. Ion Hose Instability

Potentially more disruptive than channel contraction and expansion is transverse motion caused by the ion-hose instability.^{16,20,21,38-40} This is an electrostatic instability produced as the beam and ion channel move sideways and separate. The instability convects³⁸ back from the beam head

in a characteristic growth time $\Delta\tau \sim \tau_c$ over a growth distance $\Delta z \sim \lambda_\beta/2\pi$. The instability tends to saturate as the beam offset becomes comparable to the beam and channel radii. The offset is then converted to beam emittance through phase-mixing of the particle orbits. The net effect is a centered beam but with a flared radius in the tail⁵³ (assuming there is no downstream re-excitation of the instability and $z/\lambda_\beta \geq 2\tau_p/\tau_c$). Tail flaring was in fact observed on ATA.⁸

Because an active IFR cell is typically several λ_β long, tail flaring from ion hose can be appreciable unless the pulse length is short, $\tau_p \leq \tau_c$ for initial offsets $\sim 0.1 a_b$. Ion hose can be suppressed, however, by making the channel strength $f_i I_b$ rise with time τ ; for example, the ionizing laser pulse can be made to overlap the beam pulse. A rise in $f_i I_b$ detunes the instability and, according to recent analysis to be reported in a later paper, permits pulse lengths up to $5 \tau_c$ or longer.

In a passive IFR cell, the cell length is typically $\leq \lambda_\beta$, but this is still sufficient for substantial hose growth. In this case, however, the channel strength inherently rises with τ , and the channel also follows the beam through beam ionization. Pulse lengths of $5 \tau_c$ or longer are thus permitted before ion hose and tail flaring become excessive.

C. Ion-Impact Ionization

If the ions become sufficiently energetic, they will ionize the gas. This additional ionization increases f_i , thereby altering the beam pinch force and possibly threatening the requirement that $f_i < 1$ in the beam body. Hence, ion-impact ionization should in general be minimized for IFR cells to function properly.

Ion ionization competes with beam ionization if $n_i v_{ii} \gtrsim n_b v_i$, where v_{ii} is the ion ionization rate. This can be rewritten as

$$f_i \gtrsim v_i/v_{ii} = c\sigma_b/v_i\sigma_i, \quad (54)$$

where σ_b is the beam ionization cross section, σ_i is the ion ionization cross section, and v_i is an average ion speed.

The beam ionization cross section is given from the Born-Bethe model at relativistic energies by⁵⁴

$$\sigma_b(\gamma) \approx 4\pi r_o^2 C_o Z_o [1 + C_1 \ln(\gamma)], \quad (55)$$

where $r_o = 3.86 \times 10^{-11}$ cm is the electron Compton wavelength, Z_o is the nuclear charge of the target molecule, and $C_o \gtrsim 1$ and $C_1 \approx 0.2$ are gas constants. The ion ionization cross section can be approximated using Firsov's⁵⁵ model by

$$\sigma_i(v_i) \approx 6.3 \times 10^{-15} (Z_i + Z_o)(v_i/c)(R_h/W_i) \text{ cm}^2 \quad (56a)$$

in the velocity range $5 \leq (v_i/v_o) \leq 50$. Here Z_i is the nuclear charge of the incident ion, W_i is the ionization energy, $R_h = 13.6$ eV is the Rydberg energy, and

$$v_o \approx 5.4 \times 10^{-3} (Z_i + Z_o)^{-5/3} (W_i/R_h) c \quad (56b)$$

is a scale velocity. Substituting approximations (55) and (56a) into condition (54) indicates that ion ionization becomes important when

$$f_i \gtrsim 3 \times 10^{-6} \frac{C_o Z_o}{Z_i + Z_o} (W_i/R_h)(c/v_i)^2 [1 + C_1 \ln(\gamma)] . \quad (57)$$

Energy conservation restricts the ion energy to the available electrostatic field energy:

$$\frac{1}{2} M v_i^2 \leq \frac{e(1-f_i)I_b}{c} \left(\frac{r}{a_b}\right)^2, \quad (58)$$

where $r \leq a_b$ is the starting position of the ion. Charge exchange or similar processes can reduce⁵⁶ the energy to below limit (58), but this cooling is usually unimportant at the gas densities used in IFR cells. Averaging the ion energy over both time and over all starting positions yields a mean-squared speed given by

$$\langle v_i^2 \rangle \leq e(1-f_i)I_b/2Mc, \quad (59)$$

for an ion channel initially uniform out to radius a_b .

Inserting limit (59) into condition (57) indicates that ion ionization is unimportant relative to beam ionization if

$$\begin{aligned} (1-f_i)f_i I_b &\leq 6 \times 10^{-6} \frac{C_0 Z_0}{Z_i + Z_0} (W_i/R_h)(Mc^3/e)[1 + C_1 \ln(\gamma)] \\ &\approx 0.5 Z_0 (W_i/R_h)[1 + 0.2 \ln(\gamma)] \text{ kA}. \end{aligned} \quad (60a)$$

Here we have set the ion mass M equal to $(Z_i + Z_0)$ times the proton mass, assumed $Z_i \approx Z_0$, and have set $C_0 = 2.5$ and $C_1 = 0.2$. Because Firsov's model often underestimates⁵⁵ σ_i by a factor of two, we shall impose the more restrictive requirement

$$(1-f_i)f_i I_b < (Z_0/4)(W_i/R_h)[1+0.2 \ln(\gamma)] \text{ kA}. \quad (60b)$$

This condition is always met if either $I_b < Z_0 \text{ kA}$ or $f_i I_b < Z_0/4 \text{ kA}$, for an ionization energy $W_i = 13.6 \text{ eV}$.

Condition (60b) indicates that the neglect of ion ionization is justified provided Z_0 is large and the beam current or channel strength are modest. For example, in argon ($Z_0 = 18$, $W_i = 15.8$ eV), ion ionization can be ignored if $I_b < 20$ kA or $f_i I_b < 5$ kA; using a heavier gas would raise these limits, as well as reduce other adverse effects from ion motion. Even when ion ionization is important, the increase in f_i is usually not the explosive growth described by Olson,⁵⁶ because the secondary ions are created near the beam axis where the primary ion energy is high but the electric field is low. Consequently, the secondary ions gain little field energy and thus contribute little further ionization. Note that ion and beam ionization can be eliminated altogether in an active IFR cell by operating at gas densities sufficiently low that $(\nu_i + \nu_{ii})\tau_p \ll f_i$. Condition (60b) is then not needed.

D. Trapping of Plasma Electrons

In modeling the IFR, we have assumed that the plasma electrons are instantaneously expelled to outside the beam. This is usually well justified for intense beams, unless the beam current is so high that it magnetically traps the plasma electrons. In this section, we examine magnetic trapping and the bounds it imposes on IFR propagation. A similar analysis was given by Briggs and Yu.⁴

Consider for simplicity a long beam and ion channel with identical radial profiles. The beam and channel then produce a radial electric field given by

$$E_r(r) = (1-f_i) \frac{2I_b}{r\beta_z c} i_b(r), \quad (61)$$

and an azimuthal magnetic field given by

$$B_{\theta}(r) = \frac{2I_b}{rc} i_b(r) . \quad (62)$$

Here $\beta_z c$ is the axial beam velocity, and $i_b(r)$ is the fraction of beam current within radius r .

The fields E_r and B_{θ} alter the energy and axial momentum of a plasma electron according to

$$\frac{d}{dt} (\gamma_p m c^2) = e \beta_{pr} c E_r \quad (63)$$

and

$$\frac{d}{dt} (\gamma_p m \beta_{pz} c) = e \beta_{pr} B_{\theta} , \quad (64)$$

where γ_p is the mass factor, $\beta_{pz} c$ is the axial velocity, and $\beta_{pr} c$ is the radial velocity of the electron. The total time derivative satisfies

$$\frac{d}{dt} = \beta_{pr} c \frac{\partial}{\partial r} . \quad (65)$$

Solving these equations, assuming constant f_i and I_b and zero energy initially, yields

$$\gamma_p = 1 + (1-f_i) L I_b / \beta_z I_A \quad (66)$$

and

$$\gamma_p \beta_{pz} = L I_b / I_A , \quad (67)$$

where $I_A = mc^3/e$ and

$$L(r, r') = 2 \int_r^{r'} \frac{dr''}{r''} i_b(r'') \quad (68)$$

is a dimensionless parameter related to the distributed inductance and capacitance of the beam. Here r is the initial position of the plasma electron and r' the final position.

The Lorentz condition restricts the plasma mass factor to

$$\gamma_p = (1 - \beta_{pr}^2 - \beta_{pz}^2)^{-1/2} \geq (1 - \beta_{pz}^2)^{-1/2}. \quad (69)$$

Applying this bound to Eqs. (66) and (67) produces

$$\frac{L f_i I_b}{I_A} \leq \frac{(1 - f_i) \beta_z}{1 - 0.5 f_i - 0.5 / f_i \gamma_z^2} < 1, \quad (70)$$

where $\gamma_z^2 f_i \gg 1$ is assumed implicitly and $\gamma_z = (1 - \beta_z^2)^{-1/2}$ is the beam axial Lorentz factor. A sufficient condition to expel all plasma electrons to the pipe wall at $r' = b$ is thus

$$f_i I_b \leq \frac{I_A}{2 \ln(b/a_b) + 1}, \quad (71)$$

where L has been set to its maximum value for a flat-topped beam. In practice, electrons expelled to several times a_b spend most of their time outside the beam, and they therefore have little effect on the beam. Consequently, magnetic trapping can usually be ignored for ion channel strengths $f_i I_b \leq 5$ kA.

VII. CONCLUSIONS

In this paper, we have modeled IFR cells and examined their utility for conditioning intense, relativistic electron beams. The purpose of such

conditioning is to prepare the beam for propagation through dense gas without disruption from the resistive hose instability.

Two major conditioning goals were identified: centering and emittance tailoring. Centering suppresses the hose instability by reducing the initial beam displacements that seed the instability, while tailoring reduces the hose growth rate by detuning the instability. We have found that wire-like, active IFR cells are effective at centering, and that passive IFR cells are effective at tailoring. Although both cells have been employed for these purposes, the results were often unsatisfactory and not well understood. Here we have attempted to provide a simple yet complete design procedure, and to identify the major limitations of the technique. The limitations include beam focusing from the entrance and exit foils, magnetic trapping of the plasma electrons, and ion motion in the form of channel collapse, ion hose instability, and ion ionization.

We conclude from our analysis that IFR cells are simple yet robust devices that, in a suitable parameter regime, can produce beams that are both well tailored and centered. As has already been demonstrated experimentally,^{8,27} such beams propagate much more stably through dense gas than unconditioned beams.

ACKNOWLEDGEMENTS

Many people have contributed to this analysis. In particular, we thank Richard Briggs and Simon Yu who developed the original model of the IFR and shared their work with us. In addition, we thank Frank Chambers and

William Fawley for providing information on the ATA results, Charles Frost for the Sandia results, Robert Meger and John Antoniadis for the SuperIBEX results, Glenn Joyce for the use of FRIEZR, and Martin Lampe for insights on the problem. This work was supported by the Office of Naval Research and by the Defense Advanced Research Projects Agency under ARPA Order No. 7781, monitored by the Naval Surface Warfare Center.

REFERENCES

1. W. H. Bennett, Phys. Rev. 45, 890 (1934); Phys. Rev. 98, 1594 (1955).
2. S. E. Graybill and S. V. Nablo, Appl. Phys. Lett. 8, 18 (1966).
3. See R. J. Briggs, "A Simple Model of Beam Transport in the Low Pressure Ion-Focused Regime," NTIS Document No. DE82016636, 1981.
Copies may be ordered from the National Technical Information Service, Springfield, VA 22161. The price is \$17.00 plus \$3.00 handling fee. All orders must be postpaid.
4. See R. J. Briggs and S. S. Yu, "Modeling Beam Front Dynamics at Low Gas Pressures," NTIS Document No. DE82000242, 1981. Copies may be ordered from the National Technical Information Service, Springfield, VA 22161. The price is \$12.50 plus \$3.00 handling fee. All orders must be postpaid.
5. R. J. Briggs, R. E. Hester, E. J. Lauer, E. P. Lee and R. L. Sperlein, Proceedings of the Second International Conference on High Power Electron and Ion Beam Research and Technology (Laboratory for Plasma Studies, Cornell University, Ithaca, NY, 1977), Vol. I, p. 319.
6. K. W. Struve, E. J. Lauer and F. W. Chambers, Proceedings of the Fifth International Topical Conference on High-Power Particle Beams (Lawrence Livermore National Laboratory, Livermore, CA, 1983), p. 408.
7. J. R. Smith, R. F. Schneider, M. J. Rhee, H. S. Uhm, and W. Namkung, J. Appl. Phys. 60, 4119 (1986).
8. W. M. Fawley, Bull. Am. Phys. Soc. 35, 1054 (1990).
9. J. Antoniadis, M. Myers, D. Murphy, T. Peyser, R. Hubbard, R. Fernsler, R. Pechacek and R. Meger, "IFR Cell Radius Tailoring on SUPERIBEX," Proceedings of the Eighth IEEE Pulsed Power Conference (Institute of Electrical and Electronics Engineers, New York, 1991), p. 582.

10. R. F. Lucey, Jr., R. M. Gilgenbach, J. E. Tucker, and C. L. Enloe, *Laser and Part. Beams* 6, 687 (1988).
11. R. F. Lucey, Jr., R. M. Gilgenbach, J. D. Miller, J. E. Tucker, and R. A. Bosch, *Phys. Fluids* B1, 430 (1989).
12. W. E. Martin, G. J. Caporaso, W. M. Fawley, D. Prosnitz and A. G. Cole, *Phys. Rev. Lett.* 54, 685 (1985).
13. D. S. Prono, *IEEE Trans. Nucl. Sci.* NS-32, 3144 (1985).
14. G. J. Caporaso, F. Rainer, W. E. Martin, D. S. Prono, and A. G. Cole, *Phys. Rev. Lett.* 57, 1591 (1986).
15. R. L. Carlson, S. W. Downey and D. C. Moir, *J. Appl. Phys.* 61, 12 (1987).
16. J. R. Smith, I. R. Shokair, K. W. Struve, E. Schamiloglu, P. W. Werner, and R. J. Lipinski, *IEEE Trans. Plasma Sci.* 19, 850 (1991).
17. C. A. Frost, S. L. Shope, R. B. Miller, G. T. Leifeste and C. E. Crist, *IEEE Trans. Nucl. Sci.* NS-32, 2754 (1985).
18. S. L. Shope, C. A. Frost, G. T. Leifeste, and J. W. Poukey, *Phys. Rev. Lett.* 58, 551 (1987).
19. S. L. Shope, C. A. Frost, G. T. Leifeste, C. E. Crist, P. D. Kiekel, J. W. Poukey and B. B. Godfrey, *IEEE Trans. Nucl. Sci.* NS-32, 3092 (1985).
20. K. J. O'Brien, G. W. Kamin, T. R. Lockner, J. S. Wagner, I. R. Shokair, P. D. Kiekel, I. Molin, D. J. Armistead, S. Hogeland, E. T. Powell and R. J. Lipinski, *Phys. Rev. Lett.* 60, 1278 (1988).
21. R. J. Lipinski, J. R. Smith, I. R. Shokair, K. W. Struve, P. Werner, D. J. Armistead, P. D. Kiekel, I. Molina, and S. Hogeland, *Phys. Fluids* B2, 2764 (1990).
22. M. A. Wilson, *IEEE Trans. Nucl. Sci.* NS-28, 3375 (1981).

23. B. H. Hui and Y. Y. Lau, Phys. Rev. Lett. 53, 2024 (1984).
24. P. Chen, K. Oide, A. M. Sessler, and Y. Y. Lau, Phys. Rev. Lett. 64, 1231 (1990).
25. E. J. Lauer, R. J. Briggs, T. J. Fessenden, R. E. Hester, and E. P. Lee, Phys. Fluids 21, 1344 (1978).
26. J. Antoniadis, M. Myers, D. Murphy, R. Hubbard, T. Peyser, R. Pechacek, and R. Meger, "High Current Relativistic Electron Beam Propagation in High Neutral Pressure Environments," Proceedings of the Eighth IEEE Pulsed Power Conference (Institute of Electrical and Electronics Engineers, New York, 1991), p. 585.
27. R. F. Hubbard, J. A. Antoniadis, R. F. Fernsler, M. Lampe, R. A. Meger, D. P. Murphy, M. Myers, R. Pechacek, T. A. Peyser, and S. P. Slinker, "Beam Conditioning and Propagation Experiments on SuperIBEX," to appear in Intense Microwaves and Particle Beams III, edited by H. Brandt, SPIE Conference Proceedings No. 1629 (International Society for Optical Engineering, Bellingham, WA, 1992).
28. R. F. Fernsler, R. F. Hubbard, S. P. Slinker, M. Lampe and G. Joyce, Bull. Am Phys. Soc. 35, 2083 (1990).
29. C. A. Frost, S. L. Shope, G. T. Leifeste, and D. Welch, Bull. Am. Phys. Soc. 35, 933 (1990).
30. R. F. Fernsler, M. Lampe, S. P. Slinker, and R. F. Hubbard, Bull. Am. Phys. Soc. 36, 2380 (1991).
31. R. L. Feinstein, private communication.
32. M. Lampe, R. F. Fernsler, R. F. Hubbard, and S. P. Slinker, Bull. Am. Phys. Soc. 35, 2083 (1990).
33. R. F. Hubbard, S. P. Slinker, R. F. Fernsler, M. Lampe, and G. Joyce, Bull. Am. Phys. Soc. 35, 2083 (1990).

34. C. Frost, D. Welch, and J. Wagner, private communication.
35. T. A. Peyser, J. A. Antoniadis, M. C. Myers, D. P. Murphy, R. E. Pechacek, and R. A. Meger, *Bull. Am. Phys. Soc.* 35, 2071 (1990).
36. F. W. Chambers, K. W. Struve, Y. P. Chong, and W. M. Fawley, private communication.
37. R. F. Hubbard, S. P. Slinker, R. F. Fernsler, G. Joyce, and M. Lampe, "Simulation of Electron Beam Transport in Ion-Focused Regime Conditioning Cells," submitted to *J. Appl. Phys.*
38. H. L. Buchanan, *Phys. Fluids* 30, 221 (1987).
39. K. T. Nguyen, R. F. Schneider, J. R. Smith, and H. S. Uhm, *Appl. Phys. Lett.* 50, 239 (1987).
40. S. B. Swanekamp, J. P. Holloway, T. Kammash, and R. M. Gilgenbach, *Phys. Fluids* B4, 1332 (1992).
41. S. S. Yu and R. E. Melendez, *Bull. Am. Phys. Soc.* 27, 1132 (1982); S. S. Yu, *Bull. Am. Phys. Soc.* 31, 809 (1986).
42. E. P. Lee, *Phys. Fluids* 19, 60 (1976).
43. See, for example, R. B. Miller, An Introduction to the Physics of Intense Charged Particle Beams, Plenum Press, New York (1982).
44. E. P. Lee and R. K. Cooper, *Part. Accel.* 7, 83 (1976).
45. M. Lampe, private communication.
46. See E. P. Lee and S. S. Yu, "Model of Emittance Growth in a Self-Pinched Beam," NTIS Document No. UCID18330, 1979. Copies may be ordered from the National Technical Information Service, Springfield, VA 22161. The price is \$12.50 plus \$3.00 handling fee. All orders must be postpaid.
47. See, for example, J. D. Jackson, Classical Electrodynamics, John Wiley and Sons, New York, p. 457 (1967).

48. R. J. Adler, Part. Accel. 12, 39 (1982).
49. S. Humphries, Jr., and C. Ekdahl, J. Appl. Phys. 63, 583 (1988).
50. R. F. Fernsler, R. F. Hubbard, and S. P. Slinker, J. Appl. Phys. 68, 5985 (1990).
51. W. M. Sharp and M. Lampe, Phys. Fluids 23, 2383 (1980).
52. See R. F. Fernsler and B. Hui, "Guiding of Electron Beams by Hollow Conducting Channels," NTIS Document No. ADA183693, 1987. Copies may be ordered from the National Technical Information Service, Springfield, VA 22161. The price is \$15.00 plus \$3.00 handling fee. All orders must be postpaid.
53. See J. S. Wagner and B. B. Godfrey, "BUCKSHOT Simulations of Electron Beam Transport in Rectangular IFR Channels Using ATA Parameters," NTIS Document No. DE89016670, 1989. Copies may be ordered from the National Technical Information Service, Springfield, VA 22161. The price is \$17.00 plus \$3.00 handling fee. All orders must be postpaid.
54. F. F. Rieke and W. Prepejchal, Phys. Rev. A6, (1972).
55. O. B. Firsov, J. Exptl. Theoret. Phys. (U.S.S.R.) 36, 1517 (1959), Sov. Phys. JETP 36, 1076 (1959).
56. C. L. Olson, Phys. Rev. A11, 288 (1975).
57. M. Lampe, W. M. Sharp, R. F. Hubbard, E. P. Lee, and R. J. Briggs, Phys. Fluids 27, 2921 (1984).
58. D. S. Prono, G. J. Caporaso, A. G. Cole, R. J. Briggs, Y. P. Chong, J. C. Clark, R. E. Hester, E. J. Lauer, R. L. Spoerlein, and K. W. Struve, Phys. Rev. Lett. 51, 723 (1983).
59. R. F. Fernsler and P. R. Boris, Proceedings of the Seventh International Conference on High-Power Particle Beams (Kernforschungszentrum, Karlsruhe, Germany, 1988), Vol. II, p. 900.

60. R. F. Fernsler, R. F. Hubbard, S. P. Slinker, M. Lampe, and G. Joyce,
Bull. Am. Phys. Soc. 34, 1996 (1990).
61. R. A. Meger, S. Humphries, Jr., M. Lampe, and S. P. Slinker,
Proceedings of IEEE 14th International Symposium on Discharges and
Electrical Insulation in Vacuum (Santa Fe, NM, 1990), p. 726.

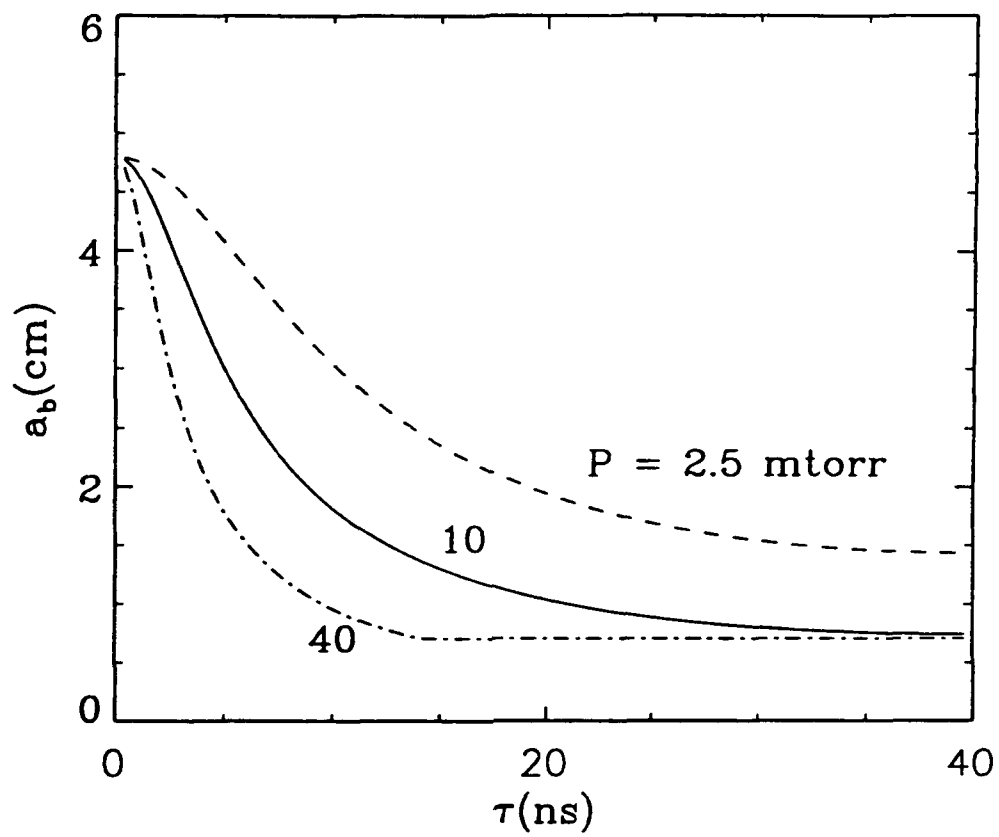


Fig. 1. Beam radius a_b as a function of τ for three different gas pressures: $P = 2.5, 10, 40$ mtorr.

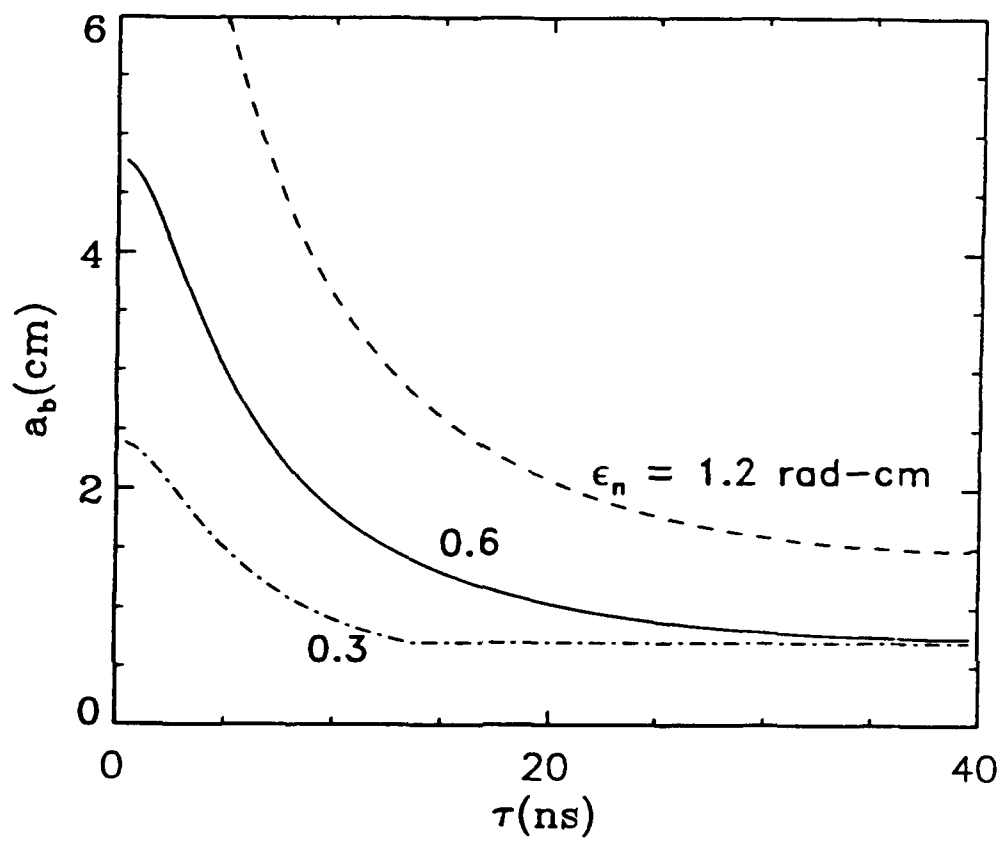


Fig. 2. Beam radius a_b for three different entrance emittances: $\epsilon_0 = 0.3$, 0.6, 1.2 rad-cm.

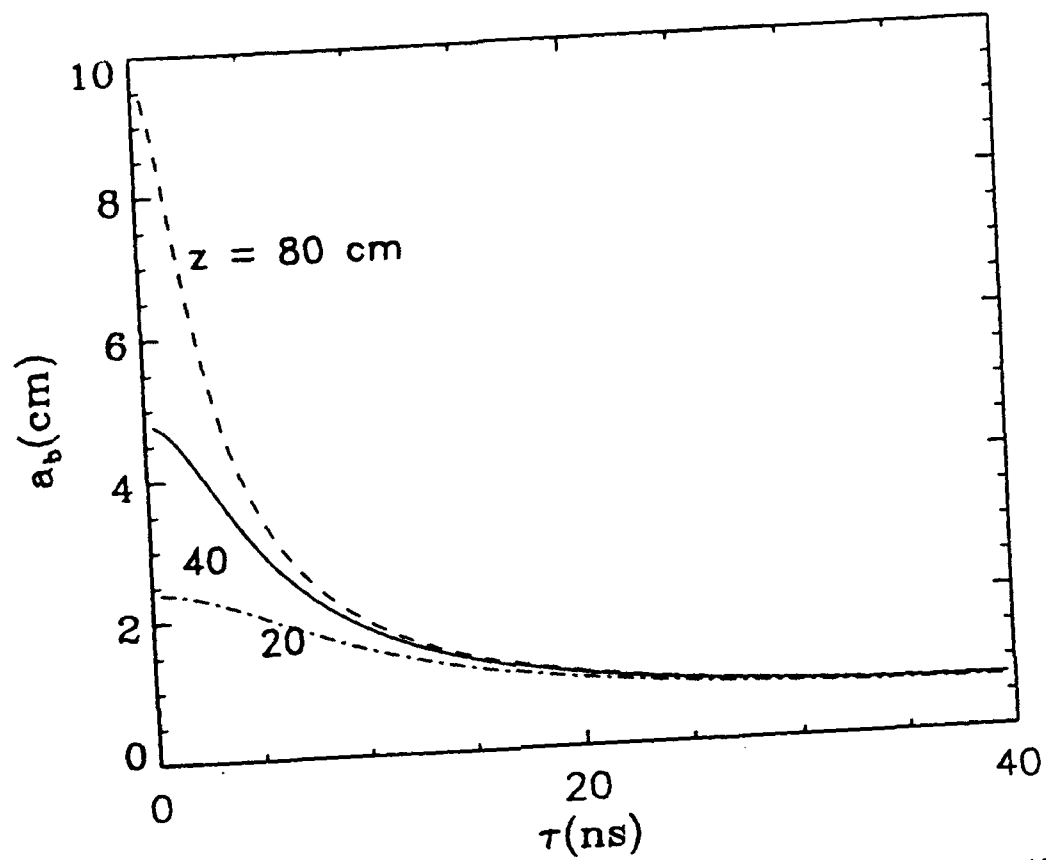


Fig. 3. Beam radius a_b for three different cell lengths: $z = 20, 40, 80$ cm.

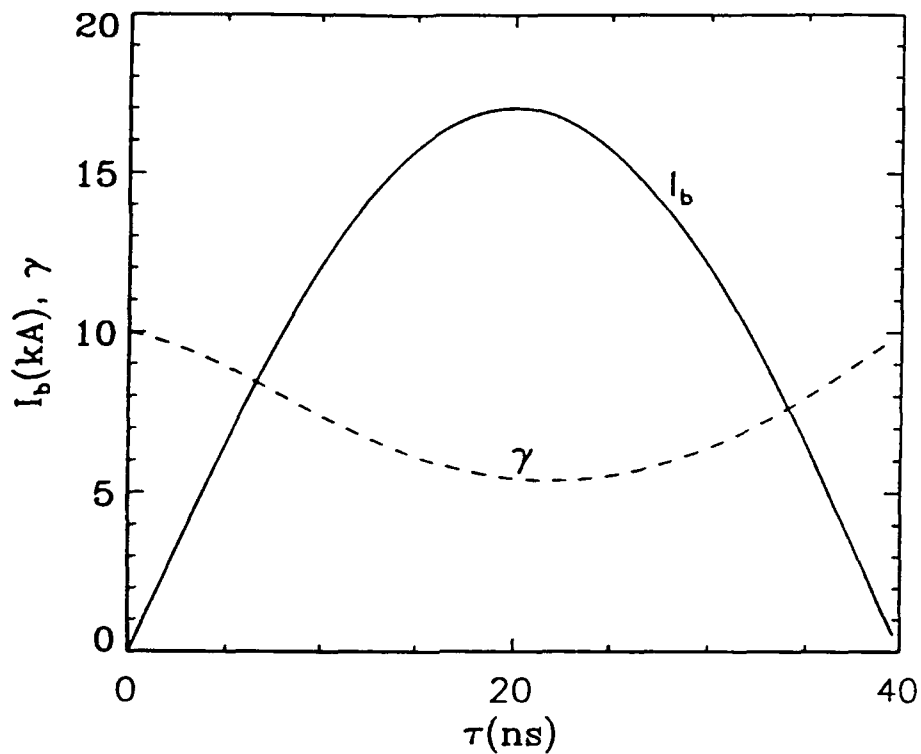


Fig. 4a. Beam current I_b and space-charge corrected energy γ as functions of τ .

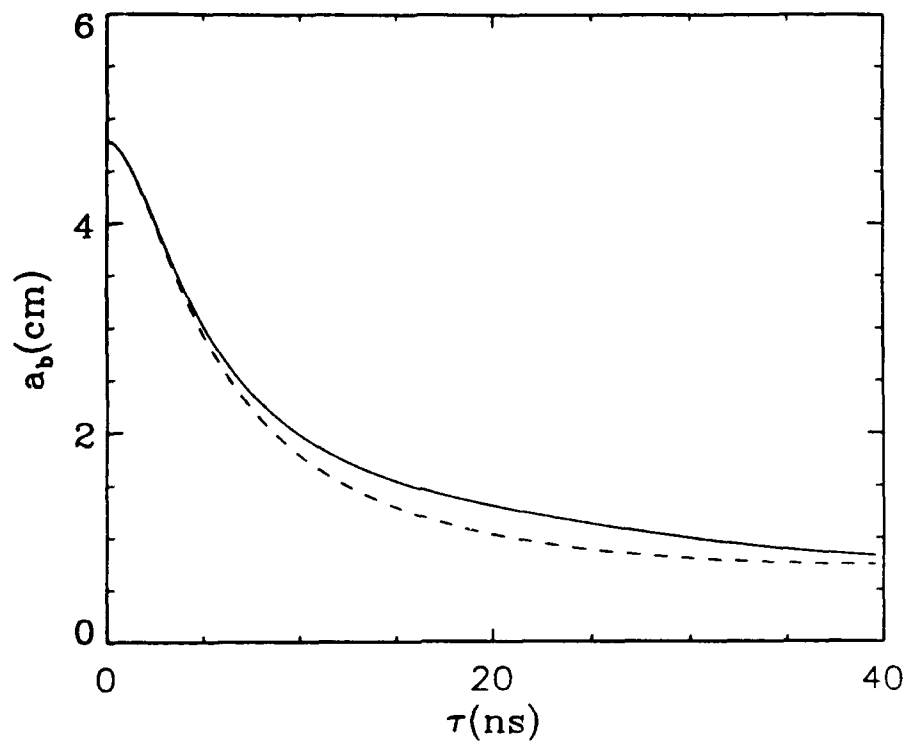


Fig. 4b. Beam radius a_b with space-charge correction (solid line) and without space-charge correction (dashed line).

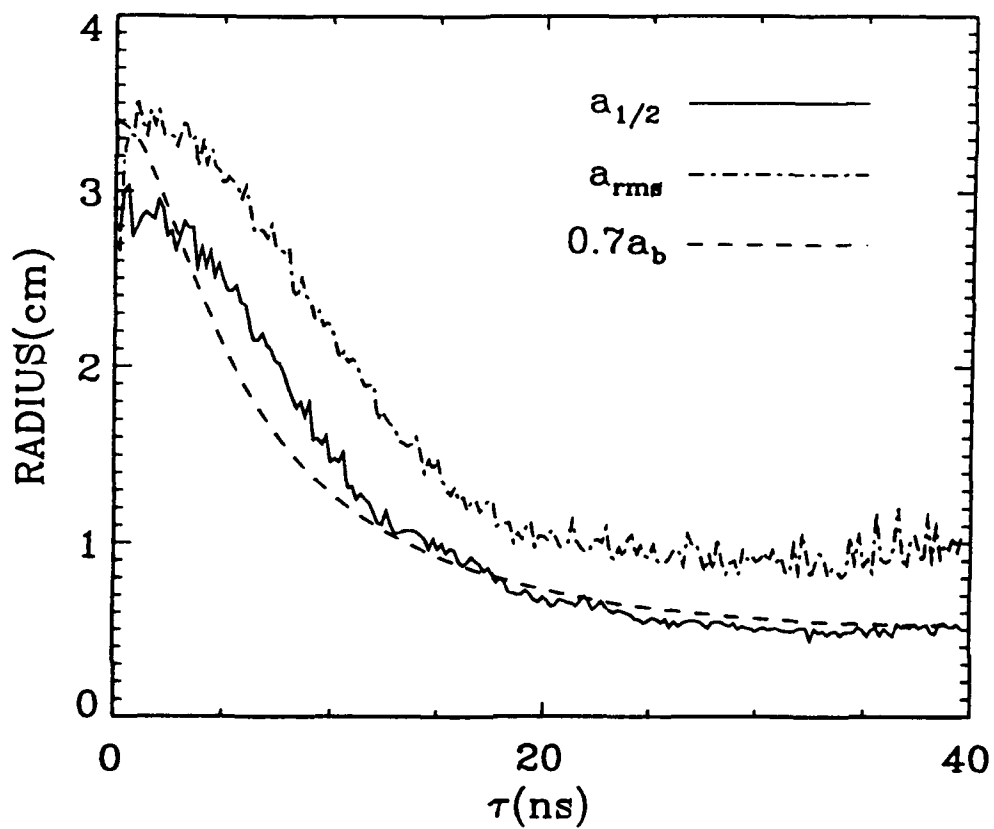


Fig. 5. Half-current radius $a_{1/2}$ (solid line) and rms radius a_{rms} (dot-dashed line) from FRIEZR, as contrasted with the analytical result $a_b/\sqrt{2}$.

APPENDIX: DETUNING THE RESISTIVE HOSE INSTABILITY

The resistive hose instability⁵⁷ is the primary factor limiting the propagation of intense, self-pinch ed electron beams in dense, un-ionized gases. Resistive hose is a macroscopic magnetic kink mode that, like the ion-hose instability in low-density gas, grows and convects back from the beam head at a rate determined by the response properties of the beam and plasma. In dense gas, the plasma response is characterized by a magnetic diffusion time τ_d proportional to the plasma conductance enclosed by the beam. The beam response is characterized by the betatron wavenumber, $k_\beta = 2\pi/\lambda_\beta$, of the beam electrons. In equilibrium,

$$k_\beta = (I_{\text{eff}}/I_A)\epsilon_n^{-1}, \quad (\text{A1})$$

where ϵ_n is the normalized beam emittance and $I_{\text{eff}} < I_b$ is the effective beam pinch current. Observe that there is no explicit dependence on beam radius a_b or energy γ in Eq. (A1).

A convective instability grows with time τ into the pulse, but it eventually decays at fixed τ (provided there is no re-excitation downstream of the accelerator). As a consequence, the hose amplitude is bounded in a pulse of finite length. Furthermore, because the amplitude scales with the initial beam displacement, the amplitude can be reduced by placing a centering cell ahead of the propagation region.^{8,26,29,36} Centering can be achieved, for example, using the active IFR cell discussed in Sec. V-B.

A second means of reducing hose growth is to "detune" the instability. Detuning is possible because^{8,30-33} the growth rate of the instability depends on the value of its oscillation wavenumber k relative to the local value of k_β . Variations in k_β with τ prevent any single frequency from

remaining in resonance throughout the pulse.

Betatron detuning occurs naturally as beam ionization causes I_{eff} to rise⁵¹ from zero with time τ . According to Eq. (A1), this detuning can be enhanced by tailoring the beam emittance ϵ_n to fall with τ . The amount of tailoring needed is dictated by the number of hose e-folds allowed. Recent hose theory²⁸ indicates that the number of e-folds varies inversely with a detuning coefficient,

$$\eta = \frac{I_{\text{eff}}}{I_b} \tau_d \frac{\partial}{\partial \tau} \ln(k_\beta) . \quad (\text{A2})$$

This coefficient is usually small because k_β for an untailored beam rises on a monopole decay time $\tau_0 \gg \tau_d$. An untailored beam can therefore suffer many orders of magnitude of hose growth. Raising the detuning parameter η by two or more through emittance tailoring can reduce hose growth dramatically.^{28,30-33}

As discussed in Sec. IV, a beam can be emittance tailored by passing it through a passive IFR cell and then through a thick exit foil or other heating mechanism. The tailoring profile, and thus the increase in η , is limited in a passive IFR cell by how rapidly the beam charge Q_b rises with τ . This restricts the amount of hose suppression possible. Other techniques proposed for tailoring include resistive wire cells,^{58,59} current-carrying wire cells,^{26,29,60} differential focusing cells,³⁷ and collapsing ion cells.⁶¹